Anodic Electrochromism for Energy-Efficient Windows: Cation/Anion-Based Surface Processes and Effects of Crystal Facets in Nickel Oxide Thin Films

Rui-Tao Wen, Claes G. Granqvist, and Gunnar A. Niklasson*

Anodic electrochromic (EC) oxides are of major interest as counter electrodes for smart window applications owing to their unique optical properties upon charge insertion and extraction. However, performance optimization of such oxides has been hampered by limited understanding of their EC mechanism, particularly in Li^+-conducting electrolytes. This paper reports on NiO_x films with $1.16 \leq x \leq 1.32$, prepared by sputter deposition. These films are immersed in an electrolyte of lithium perchlorate in propylene carbonate, and EC properties are studied by cyclic voltammetry and in situ optical transmittance measurements. The electrochromism is significantly enhanced at large values of x. It has been found that charge exchange in Ni oxide is mainly due to surface processes and involves both cations and anions from the electrolyte, which is different from the case of cathodic EC materials such as WO_3. Whereas previous studies of Ni oxide have focused on cation intercalation, the cation/anion-based mechanism presented here offers a new paradigm for designing and developing EC devices such as smart windows for energy efficient buildings.

1. Introduction

Electrochromic (EC) oxides exhibit reversible changes of their optical properties under the application of a voltage and resemble electrical batteries in that they involve joint transport of electrons and ions.[1,2] A typical device has a centrally positioned electrolyte—usually a thin inorganic film or a polymer layer—straddling two EC oxide films, and this three-layer structure is surrounded by transparent electrodes. The optical modulation is highest if one of the EC oxides colors under ion insertion (cathodically) while the other EC oxide colors under ion extraction (anodically). Specifically, the cathodic component is normally based on W oxide while the anodic part is based on Ni oxide;[1,3–5] the ions should be small in order to allow facile transport, and protons (H^+) or Li^+ are most commonly used. EC devices of this type have many applications in contemporary and forthcoming technology; the largest one, at least in terms of surface area, is in glazings for energy-efficient buildings.[4,6,7] In this case, optical transmittance modulation can be used to diminish the need for energy guzzling air conditioning and simultaneously provide a comfortable indoor environment.[8–11]

The mechanism for coloring and bleaching under charge insertion/extraction in EC oxides has been subject to numerous investigations and speculations for many years. This mechanism is rather well understood for W oxide and involves polaron absorption across a wide wavelength range centered in the near-infrared and extending over most of the luminous spectrum.[3] For Ni oxide, on the other hand, the cause of the electrochromism is much more unsettled despite the fact that scientific inquiry has persisted for almost 30 years,[12] and not only is the absorption mechanism poorly understood but even the ionic species involved in the optical modulation are sometimes ambiguous. These uncertainties are notable particularly in the case of Li^+-based electrolytes, whereas extensive work[13,14] on Ni oxide in KOH has shown that electrochromism is associated with reversible charge-transfer processes between Ni^{2+} and Ni^{3+} and can be reconciled with proton exchange in accordance with an extension of the well-established Bode reaction scheme.[15,16]

This paper reports on a detailed study of Ni oxide films in an electrolyte of lithium perchlorate in propylene carbonate ($LiClO_4$–PC). We find strong indications that the electrochromism is largely governed by surface processes, and that both cations and anions are involved in the charge exchange. The paper is organized as follows: Section 2 reviews the state of the art for understanding Li^+ exchange in Ni oxide. The composition and structure of our Ni oxide films are then described in Section 3, and electrochemical and optical properties are reported in Section 4. Section 5 contains a critical discussion of these data and their interpretation, and conclusions are drawn in Section 6. Section 7 describes the preparation and characterization of our Ni oxide films.

R.-T. Wen, Prof. C. G. Granqvist, Prof. G. A. Niklasson
Department of Engineering Sciences
The Ångström Laboratory
Uppsala University, P. O. Box 534
SE-75121 Uppsala, Sweden
E-mail: Ruitao.Wen@angstrom.uu.se

DOI: 10.1002/adfm.201500676

2. Li^+ Exchange in Ni Oxide: A Critical Assessment

The electrochromism of lithium-containing Ni oxide films has been investigated in numerous studies aimed at elucidating basic optical and electrochemical mechanisms[17–33] as well as

to produce counter electrodes for application in W oxide-based EC devices.[5,27,32,34–38]

We first consider work by Passerini et al.,[17–19,22,39] who proposed a simple two-step electrochemical reaction scheme for Li^+ insertion/extraction in sputter-deposited Ni oxide films immersed in $LiClO_4$–PC. This scheme involves an initial irreversible bleaching of the as-deposited Ni oxide by

$$NiO_x + yLi^+ + ye^- \rightarrow Li_yNiO_x \quad (1)$$

where e^- denotes electrons, followed by a reversible reaction between bleached Li_yNiO_x and colored $Li_{(y-z)}NiO_x$ as described by

$$Li_yNiO_x \leftrightarrow Li_{(y-z)}NiO_x + zLi^+ + ze^- \quad (2)$$

Hence, this scheme presumes that "activated" Li_yNiO_x is the electrochemically active material. It should be noted that the electrochemical studies of Passerini et al.[17–19] employed very low potentials, down to 1.1 V versus Li, and the initial irreversible "activation" was due to an imbalance between insertion/extraction of charge at potentials below 1.5 V versus Li. This potential range allows a number of reactions between Li, oxide materials, and electrolytes, and Li-based oxides and hydroxides can form in particular as surface layers.[40] For example, Poizot et al.[41,42] suggested that reversible formation of metal nanoparticles can occur in a matrix of Li_2O when the potential is below 2 V versus Li in accordance with

$$NiO + 2Li^+ + 2e^- \leftrightarrow Ni + Li_2O \quad (3)$$

However, such a reaction would lead to coloration of the sample due to optical absorption in Ni particles[43,44] and therefore obliterate the electrochromism. Thus, the use of working potentials below 2 V versus Li seems to be plagued with irreversible side reactions and, furthermore, is not compatible with the electrochemically reversible region of W oxide in an EC device;[3] it therefore remains questionable whether reactions (1) and (2) have any bearing on the electrochromism in a functioning device.

Campet et al.[20] put forward an alternative model for the electrochromism in Ni oxide, built on the notion that hydrogen in NiOOH migrates from the surface (surf) to the bulk according to

$$2x\,NiOOH|_{surf} + (1-2x)\,NiO|_{bulk} + 2xLi^+ + 2xe^- \rightarrow Li_{2x}Ni_{(1-x)}O|_{surf} + x\,Ni(OH)_2|_{bulk} \quad (4)$$

where NiOOH is colored and the other oxide phases are transparent. The Li-containing surface layer is then optically modulated by Li^+ insertion/extraction, and the absorption strength is governed by the Ni^{3+} concentration by

$$Li^+_{2x}Ni^{2+}_{(1-x)}O^{2-} \leftrightarrow Li^+_{(2x-y)}Ni^{2+}_{(1-x-y)}Ni^{3+}_yO^{2-} + yLi^+ + ye^- \quad (5)$$

where $Li^+_{2x}Ni^{2+}_{(1-x)}O^{2-}$ is transparent and $Li^+_{(2x-y)}Ni^{2+}_{(1-x-y)}Ni^{3+}_yO^{2-}$ is colored.

The importance of surfaces for the EC activity of Ni oxide films has been highlighted several times in connection with nonaqueous electrolytes, and it has been shown that NiO surfaces are covered by adsorbed protons and OH^- groups in the presence of very small amounts of water.[45] Specifically, hydroxide groups can be adsorbed at nickel surface sites and hydrogen at oxygen sites. As discussed by Boschloo and Hagfeldt,[24] such surface ions can be replaced by ions from the electrolyte, and it was found that the electrochemical response of sol–gel-deposited Ni oxide films was affected primarily by the type of cation in the electrolyte. Boschloo and Hagfeldt[24] interpreted their observed electrochromism as an effect of cation desorption/adsorption; cation desorption led to coloration due to electron extraction from the back contact and ensuing increased proportion of Ni^{3+} species in the film, while cation readsorption yielded bleaching.

However, qualitatively different results were observed in recent work by Mihelčič et al.[29] who investigated Ni oxide pigment coatings, prepared by spin coating, in an electrolyte of tetrabutylammonium triflate and detected adsorbed triflate ions in the colored state by ex situ infrared (IR) absorption, thus indicating that the observed electrochromism would be associated with adsorption of anions on the surfaces. In contrast, no perchlorate ions were detected in the bleached or colored states when cycling in $LiClO_4$–PC. These observations may be taken to indicate that the mechanism for optical coloration and bleaching depends on the type of electrolyte; the conclusion is provisional, however, since a rinsing procedure was performed before recording the ex situ IR spectra, which may have affected adsorbed surface species in different ways. Furthermore, Mihelčič et al.[29,46,47] observed distinct differences in IR absorption bands due to OH^- between the bleached and colored states, which may indicate that protons and/or hydroxide ions participate in the EC process. Specifically, a distinct OH^- band was observed only in the bleached state, while a broader band was seen in the colored state.[29] The intensity of the signal due to OH^-, for the bleached state, became smaller upon voltage cycling, which suggests that OH^- species are involved in the EC process mainly for the initial cycles.

It is evident from the discussion above that the electrochromism of Ni oxide films in Li^+-conducting electrolytes is a contentious subject. In order to progress toward a deeper understanding, the Ni oxide films therefore must be prepared under carefully controlled conditions and, furthermore, a well-chosen set of experiments is necessary. Specifically, our present work employs thin film fabrication by reactive DC magnetron sputtering, which minimizes contamination, and exercises detailed control of crystallinity, stoichiometry, and surface texture through a judicious selection of sputter parameters such as gas pressure, discharge power, and substrate temperature.[48,49] Films deposited on Indium-Tin Oxide (ITO) coated glass substrates were then studied by cyclic voltammetry (CV) and in situ optical transmittance measurements, as discussed below.

3. Composition and Structure of Ni Oxide Thin Films

Nickel and oxygen contents for NiO_x films were determined by Rutherford backscattering spectrometry (RBS), which yielded

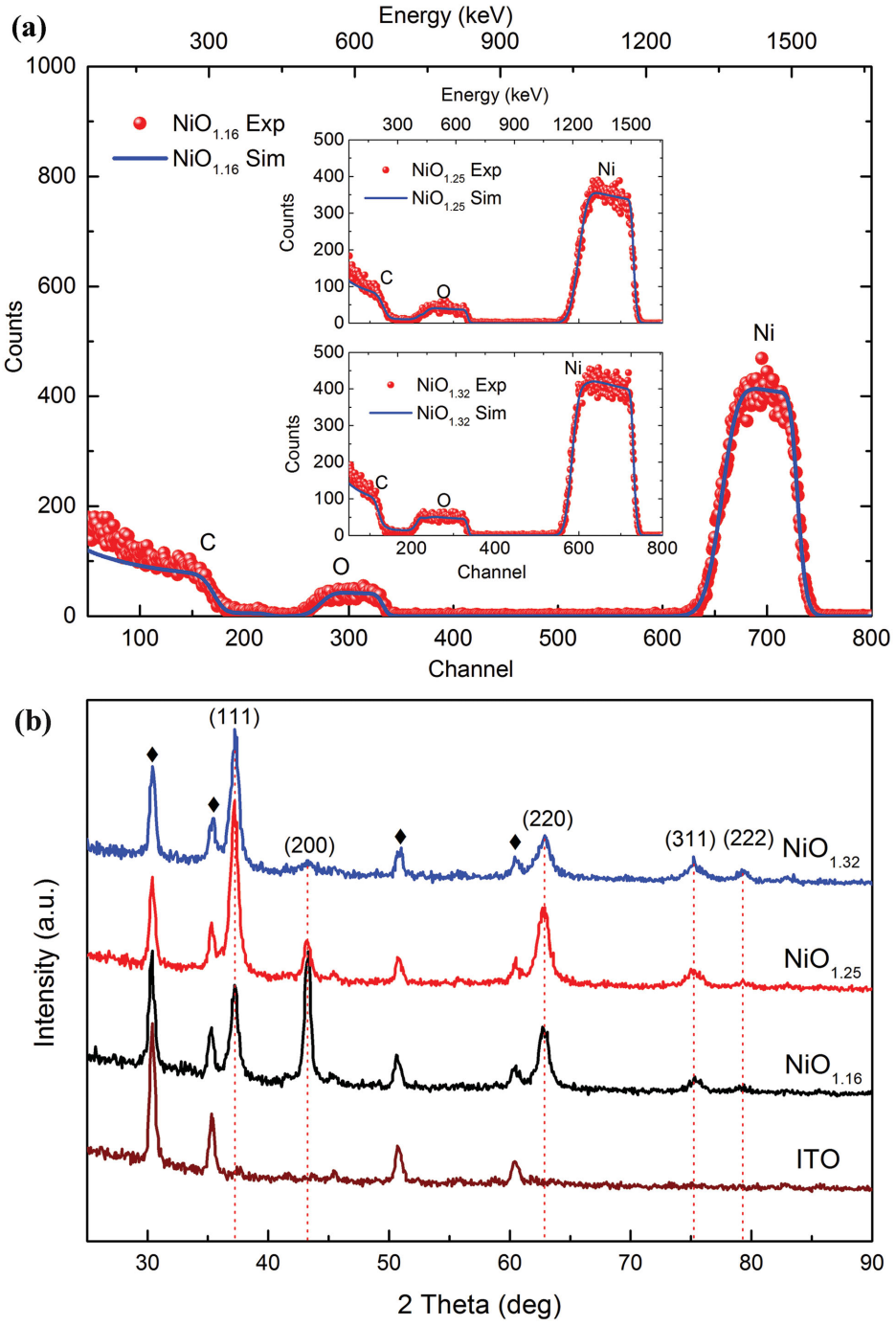

Figure 1. a) Experimental and simulated RBS spectra for Ni oxide films with the shown O/Ni atom ratios. Recorded RBS spectra were fitted to a model of the film–substrate system by use of the SIMNRA program. b) X-ray diffractograms, showing intensity in arbitrary units (a.u.) versus twice the diffraction angle, for Ni oxide films with the stated compositions and for a bare ITO/glass substrate. Dashed vertical lines show the positions of five diffraction peaks associated with NiO. Diffraction peaks indicated by diamonds at the uppermost diffractogram are due to ITO. The curves are vertically displaced.

values of x in the range $1.16 \leq x \leq 1.32$ as shown in **Figure 1**a. Hydrogen cannot be detected by RBS but probably exists in the films and/or at their surfaces. Film density ρ was calculated from RBS data and was found to be 5.0, 4.9, and 5.3 g cm^{-3} for x being 1.16, 1.25, and 1.32, respectively. Bulk NiO has a density of 6.67 g cm^{-3}.

Figure 1b displays X-ray diffraction (XRD) patterns for NiO_x films with x being 1.16, 1.25, and 1.32 as well as for an uncoated ITO/glass substrate. The films show clear evidence for NiO with cubic fcc structure (JCDPS No. 47-1049); peaks emanating from the (111), (200), (220), (311), and (222) reflections are apparent, and no evidence is found for Ni_2O_3 or any

other Ni oxide. We reiterate that a very thin layer of hydroxide may be present on the surfaces of the NiO grains but remains undetected by XRD. Crystallite sizes were estimated from Scherrer's formula[50] applied to the diffraction peak at ≈37° and were found to be ≈12.2, 11.1, and 10.8 nm for $NiO_{1.16}$, $NiO_{1.25}$, and $NiO_{1.32}$, respectively.

The relative peak heights in the diffractograms differ strongly among Ni oxide films with various values of x and signal different types of preferred orientation of the lattice planes. Thus, the $NiO_{1.16}$ film has a strong peak designated (111) and an even stronger peak for the (200) growth direction, whereas the $NiO_{1.25}$ film has reversed intensities for these peaks; these results indicate a strong transformation from (200) to (111) growth direction as x is increased from 1.16 to 1.25. Furthermore, the feature due to the (200) planes has almost vanished in the $NiO_{1.32}$ film and the (111) peak then dominates strongly, implying that most of the grains grow with (111) orientation. Our data agree with prior work which has stated several times that the (111) growth direction tends to be favored when Ni oxide films are produced in the presence of a sufficient amount of oxygen.[51–53]

Figure 2 reports scanning electron microscopy (SEM) data for NiO_x films with x being 1.16, 1.25, and 1.32 and shows that the surface features are dependent on the stoichiometry and vary from triangular shaped at $x = 1.16$ to more rod-like at $x = 1.32$. The triangular shapes are consistent with the morphology of our $NiO_{1.22}$ films reported on before.[30] The features observed in the SEM images clearly are larger than the grain sizes indicated by XRD and must consist of several grains.

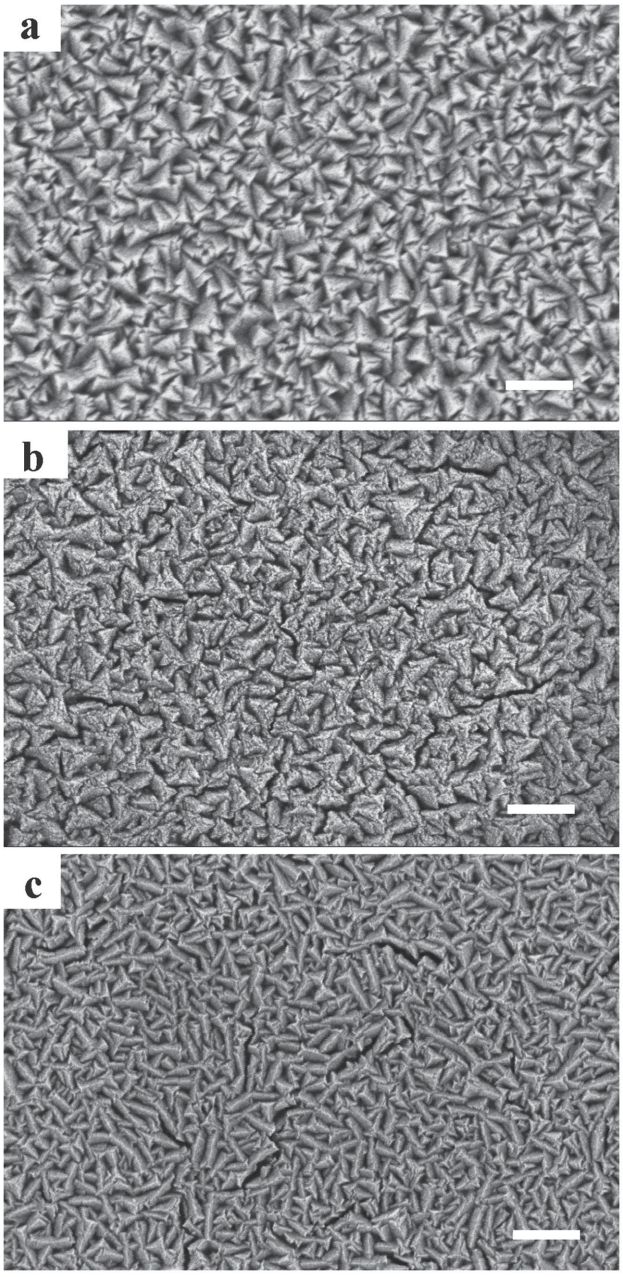

Figure 2. SEM images for films of a) $NiO_{1.16}$, b) $NiO_{1.25}$, and c) $NiO_{1.32}$. Scale bars are 200 nm in length.

4. Electrochemical and Optical Properties

4.1. Cyclic Voltammetry and Spectral Optical Transmittance

Figure 3a–c displays the first five CV scans at 2.0–4.1 V versus Li for NiO_x films with x being 1.16, 1.25, and 1.32, respectively. The cycling began at the open circuit potential (OCP) and progressed toward lower potentials. The subsequent full cycles showed qualitatively similar CV data for each of the films and indicated good electrochemical durability. The cyclic voltammograms were dependent on the value of x and, generally speaking, the charge exchange was enlarged as x was increased. A difference between the first CV cycle and the subsequent ones is noted for increasing potential from 2.0 to 4.1 V versus Li, especially for x being 1.16 and 1.25, which may be due to desorption of H^+ from oxygen sites on NiO_x as discussed in detail later. Figure 3a′–c′ reports spectral optical transmittance for the same films in initial, as-deposited state, and after coloring and bleaching corresponding to zero current density in the CV scans. The transmittance of the as-deposited films were lower the larger the oxygen content, which can be reconciled with a higher proportion of Ni^{3+} sites and a larger amount of Ni vacancies. During the first voltammetric half-cycle from the OCP and toward 2.0 V versus Li, the optical transmittance changes from the initial condition to a bleached state with significantly higher transmittance, and coloration then takes place as the potential is swept toward 4.1 V versus Li. It is important to note that the transmittance in the stabilized, colored (bleached) state is lower (higher) than that of the as-deposited sample. The colored-state transmittance is also progressively lower in films with increased values of x. Films with small oxygen content showed high as-deposited and bleached-state transmittance and the coloration was rather modest; films with higher oxygen content, on the other hand, showed lower bleached-state transmittance but larger optical modulation.

In the previous data, the cyclic voltammograms were recorded as the voltage was initially swept from the OCP toward the lower potential limit at 2.0 V versus Li with ensuing bleaching of the sample. Alternatively, the initial half-cycle can progress from the OCP toward the upper potential limit at

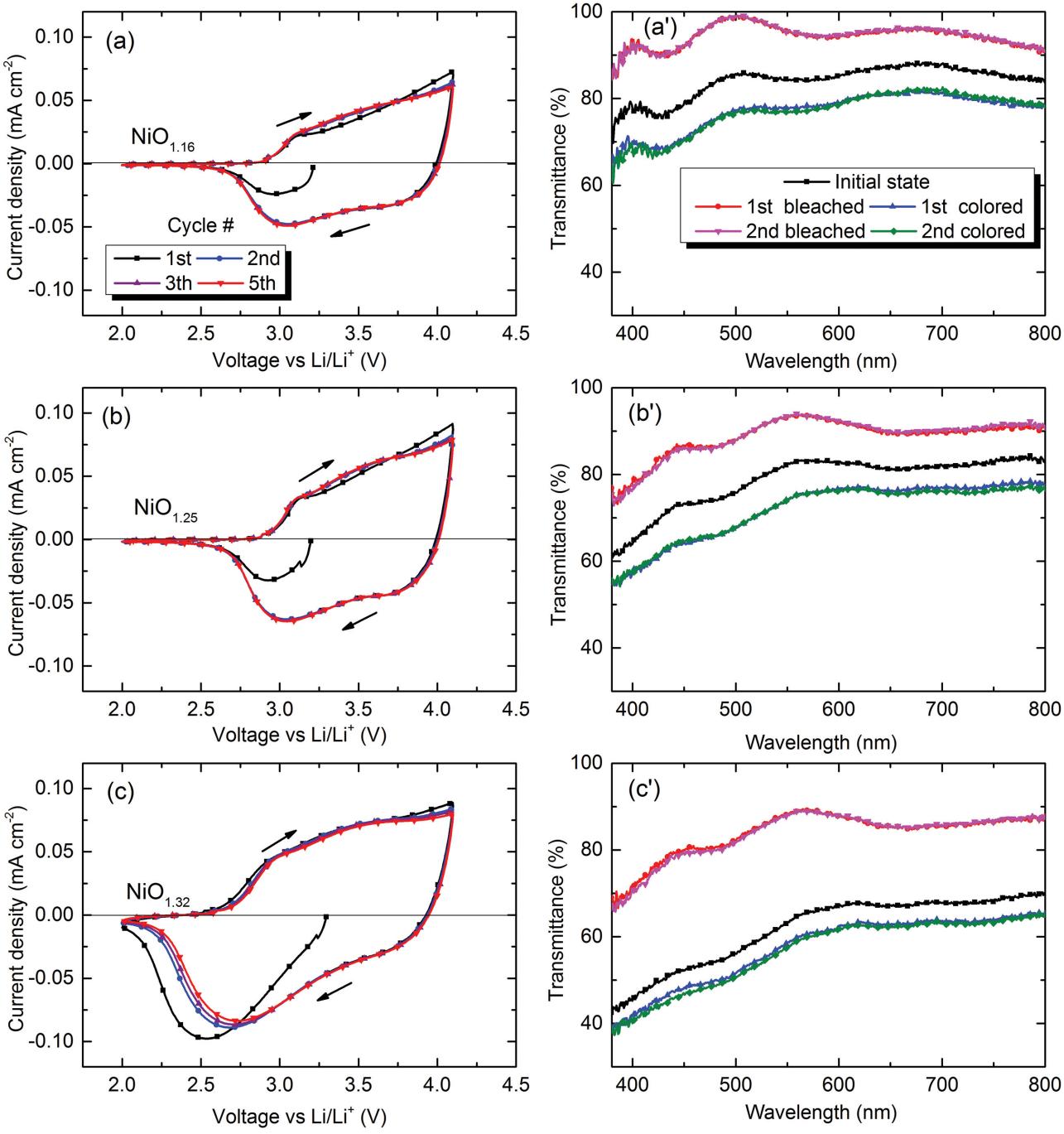

Figure 3. Cyclic voltammograms and spectral transmittance for Ni oxide films with the shown compositions immersed in $LiClO_4$–PC. Voltammograms in (a–c) were recorded for the indicated number of cycles at 50 mV s^{-1}; arrows denote sweep direction. Corresponding spectral optical transmittance data in panels (a′–c′) were taken for films in as-deposited state and at full coloration and bleaching after the first and second voltage scan.

4.1 V versus Li. **Figure 4** shows a comparison of data obtained in the different manners for a Ni oxide film with $x = 1.16$. The film displays almost the same charge insertion and extraction properties after the first CV cycle and identical stable coloration and bleaching in both cases. Importantly, the optical transmittance increases during the initial scan from OCP to 2 V versus Li (Figure 4c, inset) and decreases during the initial CV scan from the OCP to 4.1 V versus Li (Figure 4d, inset). Clearly, the Ni oxide can be bleached or colored from the as-deposited state depending on voltage scan direction.

Figure 5 elaborates the role of the upper potential window, denoted U_H, for the electrochemical and optical properties of NiO_x films. Figure 5a–c refers to the second, electrochemically stabilized, CV cycle for films with x being 1.16, 1.25, and 1.32,

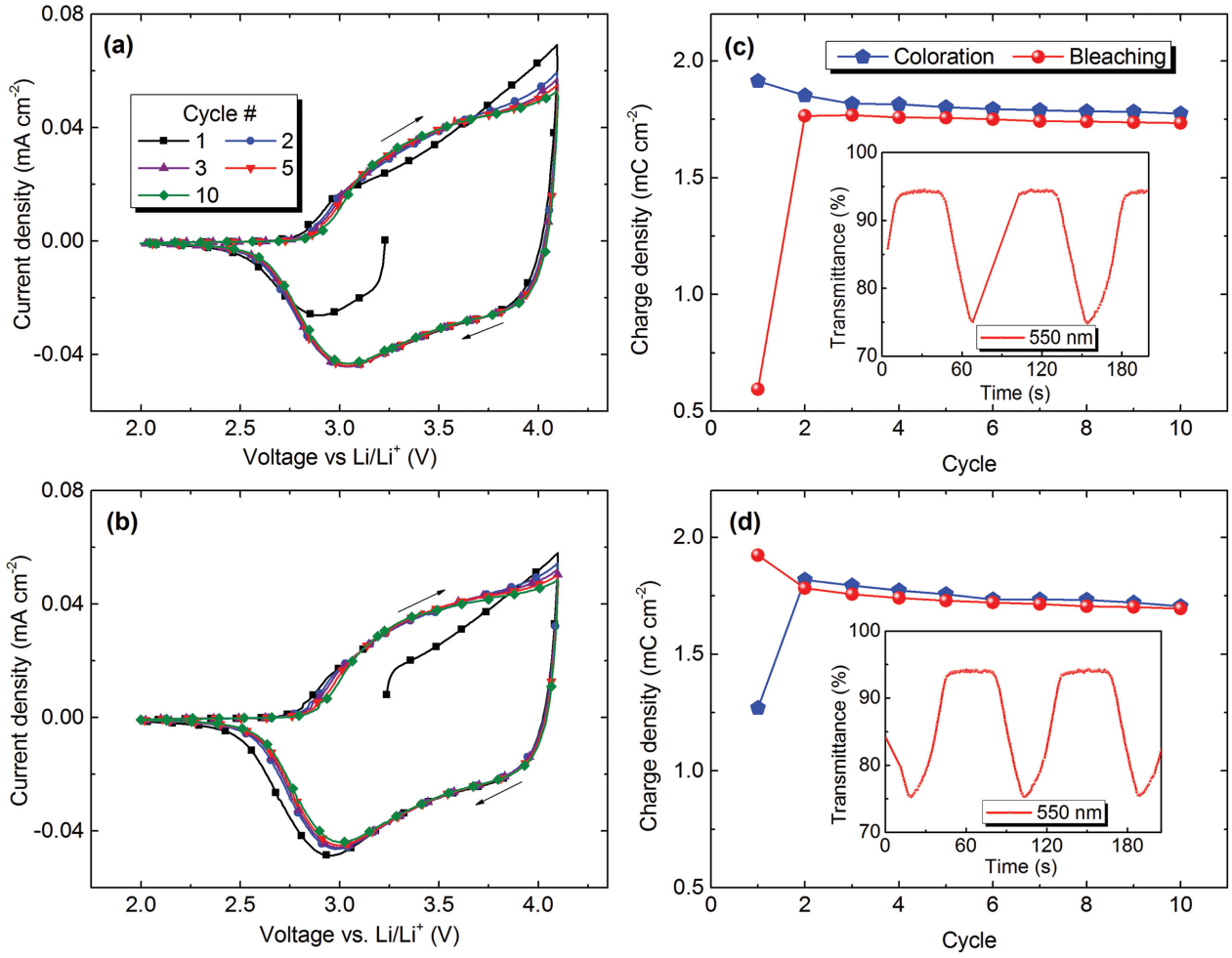

Figure 4. a,b) Cyclic voltammograms for an $NiO_{1.16}$ film immersed in $LiClO_4$–PC. Data were recorded for the indicated number of cycles at 50 mV s^{-1}; arrows denote sweep direction. The first cycle starts from the OCP and progresses toward a) low and b) high voltage, respectively. c,d) Charge density obtained from CV data in (a) and (b); insets in (c) and (d) indicate optical transmittance at 550 nm.

respectively. U_H was set at four values from 3.7 to 4.7 V versus Li and, expectedly, the charge exchange is markedly increased in proportion to the magnitude of U_H. Charge exchange takes place in a wider potential range when the oxygen content is increased in NiO_x. Figure 5a′–c′ shows that all of the films have a transmittance around 90% at a mid-luminous (550 nm) wavelength irrespectively of the width of the potential window. For x = 1.16, the film colored by sweeping the potential to U_H = 3.7 V versus Li has almost the same optical properties as in the as-deposited state, whereas films characterized by x being 1.25 and 1.32 were then somewhat more transparent than in their corresponding as-deposited states. The optical modulation span becomes greater as U_H is enlarged and also—to an even larger extent—as x is increased; in other words, large oxygen content is conducive to electrochromism.

Charge insertion/extraction as a function of cycle number is illustrated in detail in **Figure 6** for three types of Ni oxide films and in four potential windows. The charge exchange during the first bleaching is in most cases considerably less than in subsequent cycles, as also inferred from the CV data in Figures 3–5. Extended CV cycling leads to a slow and monotonic decrease of the charge densities for coloring and bleaching; the fall-off takes place at a rate that levels off as the cycle number progresses. This behavior is in qualitative agreement with a power-law decay reported for Ni oxide films cycled for up to 10^4 times in earlier work of ours.[30] With one clear exception (Figure 6i), the charge for coloration is somewhat larger than that for bleaching after the first CV cycle. The charge exchange is enhanced for increased values of x and U_H.

4.2. Fractal Dimension of the Films' Surface Structure

The Ni oxide films have very uneven surfaces, as apparent from the SEM data in Figure 2, and it is important for our analysis below that this roughness is quantified, which can be done by use of a fractal dimension d_f for the surface. We extracted d_f by taking CV data at different voltage sweep rates by use of the Randles–Sevčik (R–S) equation[54,55] or its fractal generalization.[56–58]

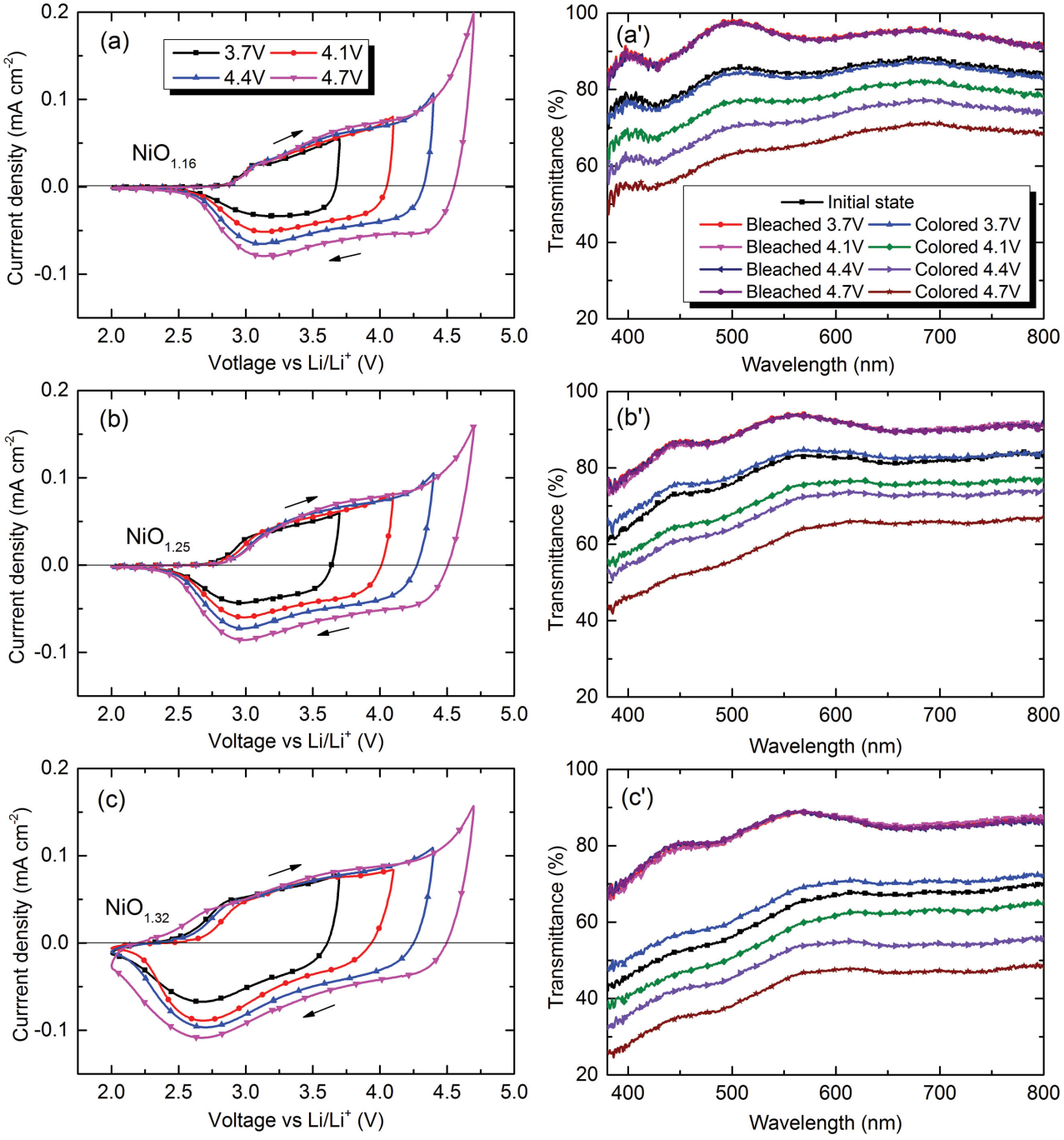

Figure 5. Cyclic voltammograms and spectral transmittance taken at the second voltammetric cycle for Ni oxide films with the shown compositions immersed in $LiClO_4$–PC. Voltammograms, shown in panels (a–c), were recorded for cycling to the indicated values of the upper potential limit at 50 mV s^{-1}; arrows denote sweep direction. Corresponding transmittance data, shown in panels (a′–c′), were taken for films in as-deposited state and at full coloration and bleaching.

Figure 7a reports CV scans obtained by using sweep rates from 2 to 100 mV s^{-1} for a film with $x = 1.16$. These data consistently show one pronounced peak in (negative) current density (I) during the sweep toward lower potentials. The peak current was found to depend as a power law on sweep rate, as seen in Figure 7b, which also shows data for films with $x = 1.25$ and $x = 1.32$. The fractal generalization of the R–S equation gives that the power-law exponent α is related to the fractal dimension as

$$\alpha = (d_f - 1)/2 \quad (6)$$

which yields d_f values in the narrow range 2.80 ± 0.06.

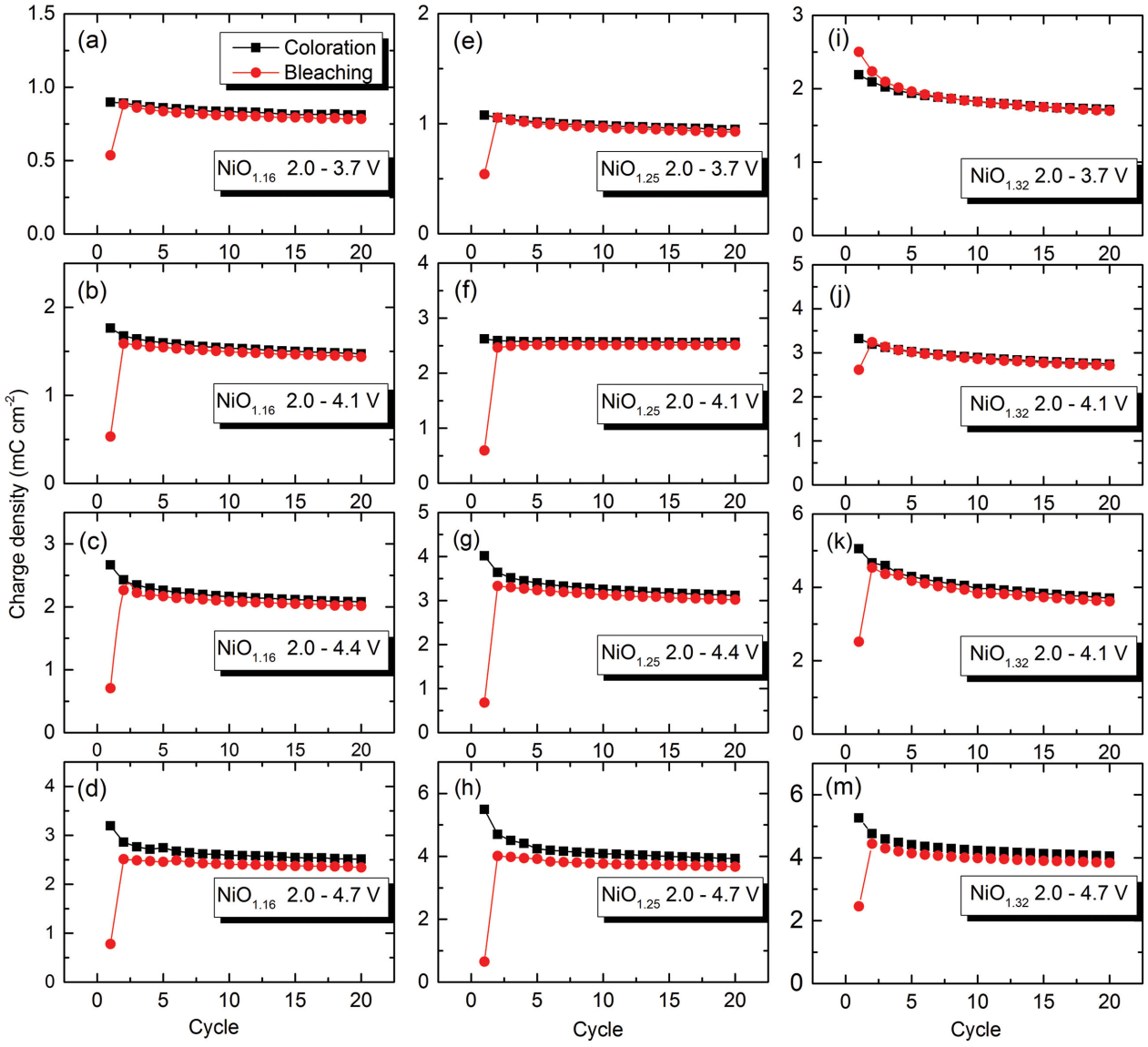

Figure 6. Exchanged charge density during bleaching and coloring versus voltammetric cycle number for Ni oxide films with the shown compositions immersed in $LiClO_4$–PC and cycled at 50 mV s^{-1} in the shown potential windows. Note that the vertical scales are different among the various panels.

5. Discussion

5.1. Electrochemical Reactions are Surface Processes

We first consider the oxygen excess in the as-deposited Ni oxide films, which were produced by sputtering in pure oxygen–argon plasma. H^+ and OH^- can adsorb on the NiO surface when the film is exposed to ambient atmosphere.[45] Hence, it is plausible that some hydroxide and oxyhydroxide species are present on the surfaces, and it is often assumed[13,14] that Ni oxide films with EC properties consist of NiO grains with outer layers of $Ni(OH)_2$ and NiOOH. In transparent films, the oxygen excess must be due exclusively to $Ni(OH)_2$ whereas absorbing films must contain NiOOH and/or Ni_2O_3; the latter species is likely to be hydroxylated upon exposure to ambient air, at least if present on a surface.

Both $Ni(OH)_2$ and NiOOH can be represented as $NiO_{(1+\gamma)}$ with $\gamma = 1$, and Ni_2O_3 has $\gamma = 0.5$, whereas our films are characterized by $0.16 \leq \gamma \leq 0.32$, and it is interesting to contemplate where the (oxy)hydroxide (or dinickel trioxide) is located in our samples. To this end we first estimate the surface/volume ratio $(S/V)_g$ of NiO grains assuming that they are spherical with radius R and have a surface layer thickness ΔR, so that $(S/V)_g = 3\Delta R/R$. Setting ΔR = 0.42 nm, corresponding to one lattice constant in NiO, and $2R$ = 12 nm to be consistent with the grain size inferred from XRD data in Figure 1b, we obtain $(S/V)_g = 0.21$. This is of the same order of magnitude as the oxygen excess in our samples and indicates that the species contributing to the oxygen excess are present as thin layers at grain boundaries.

How much of the oxygen excess in our films is due to $Ni(OH)_2$ and how much to the absorbing species? The films

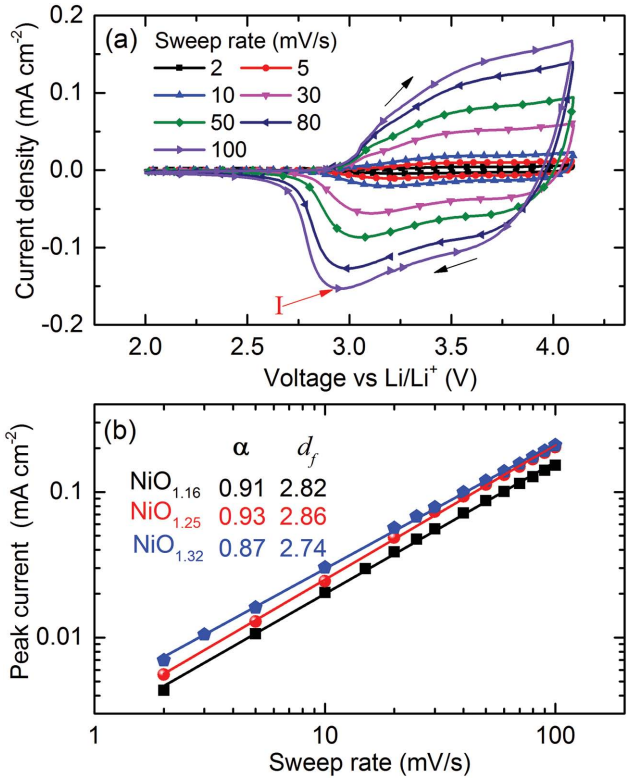

Figure 7. Determination of fractal dimension d_f for Ni oxide film surfaces. a) CV curves for an $NiO_{1.16}$ film at the shown voltage sweep rates; the current at the arrow (denoted *I*) was used to evaluate d_f. b) Peak current, extracted from voltammograms such as the one in (a), versus potential scan rate for NiO_x films with the shown values of *x*. The parameter α was obtained from a power-law fit to the data points, which then yielded d_f.

were almost completely bleached during the initial voltammetric half-cycle toward low potentials (cf. Figure 4), and the charge exchange per area unit (Q/A) during this half-cycle allows an estimate the number q of exchanged monovalent ions per Ni atom from

$$q = \left(M_{\mathrm{mol}} / ed\rho N_{\mathrm{A}}\right)\cdot\left(Q / A\right) \tag{7}$$

where M_{mol} is molar mass of NiO, d is film thickness, and N_{A} is Avogadro's constant. From Figure 6, the charge density after the first bleaching corresponds to a charge exchange of 0.5–0.7 mC cm^{-2} for films with $\gamma = 0.16$ and $\gamma = 0.25$, and of ≈2.5 mC cm^{-2} for $\gamma = 0.32$. Using $\rho \approx 5.0$ g cm^{-3}, one finds corresponding q values of ≈0.003 and ≈0.011.

At face value, the smallness of this parameter indicates that the majority of the oxygen excess in our films would be due to $Ni(OH)_2$, and it is highly probable that absorbing species exist only on the film surface, i.e., where reactions with the ions of the electrolyte are most facile. However, the analysis can be refined, and we therefore introduce a $(S/V)_f$ ratio for the film, whose minimum value is $\approx \Delta R/d$, i.e., ≈0.0014 in the present case. We recall that the film surfaces are rough (cf. Figure 2), and an "amplification factor" for $(S/V)_f$ can be estimated from the fractal dimension estimated from the data in Figure 7. We assume that the inner cutoff for the fractal structure is equal to the lattice constant and that the outer cutoff (correlation length ξ) is equal to the radial size of the features seen in Figure 2, i.e., ≈20 nm. The area of a flat surface scales as r^2 and the area of a fractal surface scales as r_f^d, where r is a distance on the surface. Hence, the "amplification factor" is $\approx(\xi/\Delta R)^{(d_f - 2)}$, where r was replaced by the ratio between the correlation length and the lattice constant. The enhancement factor does not appear to have any clear dependence on the composition parameter x. Our estimated $(S/V)_f$ ratio then becomes ≈0.03, which is much higher than q, but it must be borne in mind that this is an order-of-magnitude estimate only. Nevertheless, our estimate is clearly consistent with the assumption that the absorbing species are confined to the surface of the Ni oxide films. Furthermore, it is interesting to note that the maximum coloration charge, observed in Figure 6 for the upper potential limit 4.7 V versus Li, translates to $q \approx 0.024$, which is in very good agreement with our estimate. Our results hence indicate that the whole surface area is fully occupied by absorbing species only at high applied potentials.

5.2. Crystal Facets are Important for Strong Electrochromic Coloration

We now consider the relation between, on one hand, the degree of optical absorption and the possible species adsorbed on the surface and, on the other hand, the different preferential orientations of the films as evidenced in Figure 1b where we emphasized the roles of the (111) and the (200) crystal facets. As illustrated in **Figure 8**, the (111) planes in NiO are terminated by Ni atoms, while the (200) planes are terminated by both oxygen and nickel atoms.[45,59] Importantly, these two types of planes have different abilities to adsorb cations and anions; when NiO films are exposed to the atmosphere, OH^- ions are adsorbed on the Ni sites and H^+ ions on the O sites of the surface. According to Boschloo and Hagfeldt[24] the metal sites attain the charge state Ni^{2+} in the case of equal amounts of the two adsorbed species. It should be noted that the (111) planes have the highest density of atomic sites and that, under ambient conditions, it is easier to adsorb OH^- on the exposed Ni sites than protons to the underlying O sites, the net result leading to the formation of NiOOH and yielding low optical transmittance in the initial state. Cappus[45] also experimentally found a higher proportion of OH^- adsorption on the (111) surface than on the (200) surface of NiO.

How can the observations above account for the differences in optical absorption for the various as-deposited NiO_x films? Optical absorption would be due to an excess of adsorbed OH^-, compared to the amount of adsorbed H^+,[24] and lead to the formation of Ni^{3+} sites, which would be most likely on the (111) planes since their O atoms lie below the Ni atoms and hence are less accessible. The comparatively strong optical modulation for $NiO_{1.32}$ would then be due to the abovementioned effect and ensue from an additional contribution due to the small interatomic distances in the (111) plane. All of the Ni oxide films were almost completely bleached during the initial half-cycle, most probably as a consequence of desorption of OH^- from easily accessible Ni sites on the surface. Instead going from the as-deposited state to the colored state in the initial voltammetric

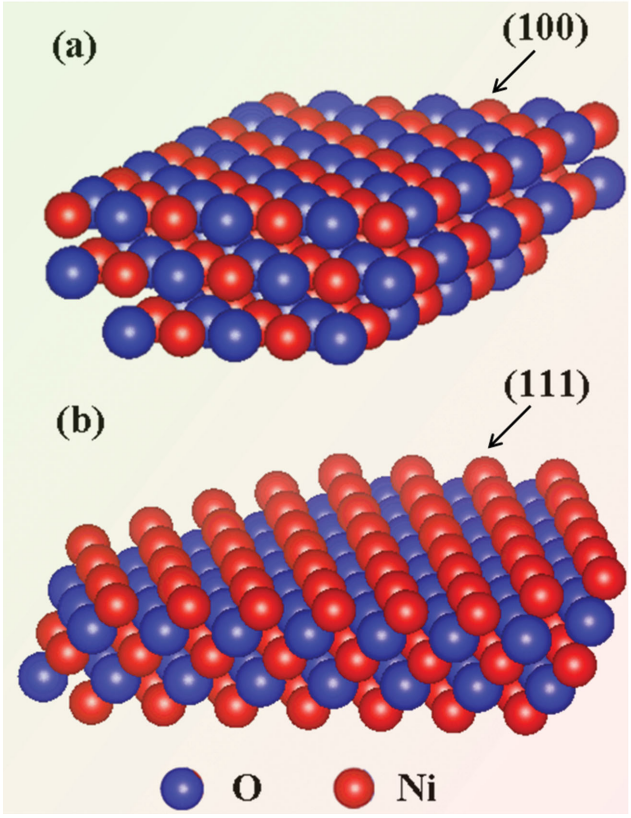

Figure 8. a) (100) plane of fcc NiO; oxygen and nickel atoms are in the same plane and exposed equally to air. b) (111) plane of fcc NiO; oxygen atoms and nickel atoms are not in the same plane, and nickel atoms are predominantly exposed to air.

half-cycle, protons can be desorbed and give increased optical absorption. However, adsorption of anions from the electrolyte onto less accessible Ni sites may also contribute, at least at high potentials.

The most oxygen-rich film, $NiO_{1.32}$, shows the largest charge exchange and yields the largest optical modulation, which is consistent with the arguments above. This film also displays the largest optical variation from initial state to bleached state. These features are probably due to the film's large proportion of Ni sites on the exposed (111) planes. Correspondingly, oxygen atoms are less exposed; this implies that few protons are present initially and amenable to desorption, which results in a small optical difference between the initial state and colored state at potentials below 4.1 V versus Li. The increased optical absorption at higher voltages should, at least partly, be due to adsorption of anions from the electrolyte.

The case is different for films of $NiO_{1.25}$ and $NiO_{1.16}$, however, since they have strong XRD reflections due to both (111) and (200) planes, which indicates a smaller difference in the number of exposed oxygen and nickel atoms. The optical absorption in the as-deposited films is lower than for $NiO_{1.32}$, as apparent from Figure 5, and is due to the difference of adsorbed OH^- and protons on easily accessible surface sites. The variation of optical absorption from the initial state to both bleached and colored states is similar at the upper potential, 4.1 V versus Li. The decreased colored-state transmittance at higher potentials is believed to be due to a combination of proton desorption and of adsorption of anions from the electrolyte. Thus, we conclude that the degree of optical absorption in the as-deposited films, as well as the achievable contrast between bleached and colored states, is determined by exposed crystallographic planes. The initial bleaching of the films reported on in Figure 4a can then be understood as a result of OH^- ion desorption from the surface, while the initial coloring of the film reported on in Figure 4b is at least partly due to H^+ ion desorption.

Considering next the coloration–bleaching mechanism in subsequent cycles, it is unlikely that the coloration of the Ni oxide films following the first bleaching is caused solely by the adsorption of anions, irrespectively of them being OH^- or ClO_4^-. Since the charge exchange during the first coloration is larger than during the initial bleaching, desorption of cations should also contribute. The same argument can be applied to the bleaching after the first coloration in Figure 4b. We also note that the charge density during the first coloration (1.91 mC cm^{-2}) in Figure 4a is slightly larger than the sum of the initial half-cycles in Figure 4a,b (0.59 + 1.27 = 1.86 mC cm^{-2}), which may suggest that the first coloration is due not only to adsorption of OH^- and desorption of protons but that ions of the electrolyte contribute.

Hence, we propose that the coloration/bleaching processes after the first half-cycle are due to a combination of cation and anion exchange. Desorption of cations and adsorption of anions leads to extraction of electrons from the back contact (the ITO layer) whereby the film colors, and the opposite processes occur during bleaching. In addition, after the first cycle the importance of proton and hydroxide exchange gradually decreases and it is mainly the ions in the electrolyte that will take part in the adsorption/desorption processes at the surface. This interpretation is consistent with the observation of ex situ spectroelectrochemical results of Orel and co-workers which showed that OH^- signatures became progressively less prominent upon CV cycling during the first few cycles for NiO_x films.[29,60] The adsorption of Li^+ and ClO_4^- will, in the absence of side reactions, eventually prevail.

By analyzing correlations between the colored state and the upper potential limit, we found that the charge exchange is markedly enhanced as U_H is increased from 3.7 to 4.7 V versus Li (Figure 5a–c), thereby yielding a lowered transmittance in the colored state (Figure 5a′–c′). This result indicates that there are surface sites with a broad distribution of adsorption and desorption energies, and that less accessible sites need a higher potential to take part in the processes.

We finally note that Figure 6 reports that, with some exception, the charge for coloration is somewhat larger than that for bleaching. This difference points at a small irreversibility in the adsorption and/or desorption process, and it seems that all inserted anions cannot be extracted. This small irreversibility leads to a minor gradual decrease in the charge capacity. However Figure 6i, pertaining to the most oxygen-rich film and the smallest potential window (2.0–3.7 V vs Li), is qualitatively different; this figure shows that the charge exchange for bleaching is larger than for coloring in the first cycles, and one can observe that the bleached state has higher transmittance than in the initial state, thus indicating that the initial

desorption of anions has not all been compensated by adsorption at 3.7 V versus Li. However, after a few cycles the coloration and bleaching charge densities exhibit the same behavior as for the other cases in Figure 6.

6. Conclusion

We presented results from a comprehensive study of well-characterized sputter-deposited Ni oxide films immersed in a $LiClO_4$–PC electrolyte. Cyclic voltammetry and in situ spectral optical transmittance were recorded for NiO_x films with $1.16 \leq x \leq 1.32$, and it was found that the optical modulation range was enhanced as x was increased and as the potential window for voltammetric cycling was enlarged. These films had different preferred orientations, which were found to be related to the achievable degree of coloration and hence very significant for the electrochromic properties. Furthermore, our data are consistent with a model assuming that both cations and anions contribute to the charge exchange—and hence the electrochromism—and that these ions partake in surface reactions rather than processes in the bulk.

Our work has led to a refined conceptual framework for discussing the electrochromism of Ni oxide in contact with Li^+-conducting electrolytes, which thus far has been an elusive topic and subject to speculations for many years. Our new model may also turn out to be useful for understanding ageing and degradation of EC devices incorporating Ni oxide, which is an important topic for smart windows in energy efficient buildings.

7. Experimental Section

Thin Film Deposition: The Ni oxide films were deposited by reactive DC magnetron sputtering in a coating system based on a Balzers UTT 400 unit as described in detail elsewhere.[30] The sputtering chamber contained 30 mTorr of argon and oxygen gas, and films of NiO_x with $1.16 \leq x \leq 1.32$ were prepared by varying the O_2/Ar ratio from 2.0% to 10%. These films were deposited onto unheated substrates of ITO-coated glass for EC measurements and simultaneously onto carbon plates for compositional determinations. The ITO (i.e., In_2O_3:Sn) layer had a sheet resistance of 60 Ω. Substrate rotation during sputter deposition ensured film uniformity. The film thickness was determined to be 280–300 nm by surface profilometry using a Dektak XT instrument. Films deposited with successively larger O_2 contents in the sputter plasma had a progressively more brownish appearance.

Compositional Characterization: Nickel and oxygen contents were determined by Rutherford backscattering spectrometry at the Uppsala Tandem Laboratory, using 2 MeV ^{4}He ions backscattered at an angle of 170°. The RBS spectra were fitted to a model for the film–substrate system by use of the SIMNRA program.[61]

Structural and Morphological Characterization: Film crystallinity was investigated by X-ray diffraction using a Siemens D5000 diffractometer with CuKα radiation at a wavelength of 0.154 nm. Structure and phase composition were obtained by comparison with the Joint Commission of Powder Diffraction Standards (JCPDS) database. Film morphology was characterized by scanning electron microscopy using a LEO 1550 FED Gemini instrument with an acceleration voltage of 10–15 kV.

Electrochemical and Optical Properties Measurements: Cyclic voltammetry was carried out in a conventional three-electrode cell by use of a computer-controlled ECO Autolab/GPES Interface. The whole measurement was conducted in an argon-filled glove box with a water content of ≈0.5 ppm. A Ni oxide film served as working electrode and was immersed in an electrolyte of 1 M $LiClO_4$ in PC. Both counter electrode and reference electrode were Li foils. The voltage was normally swept at 50 mV s^{-1} in the range between a low potential of 2.0 V versus Li and a high voltage set in the range 3.7–4.7 V versus Li; the arrangements and settings are consistent with those in earlier work of ours.[30,31,62] Charge capacity determined from CV data is given by

$$C = \int \frac{jdV}{s} \tag{8}$$

where C is charge capacity (mC cm^{-2}), j is current density (mA cm^{-2}), s is scan rate (V s^{-1}), and V is voltage (in V). Spectral optical transmittance was recorded in situ in the 380–800 nm wavelength range (corresponding to luminous radiation) during electrochemical cycling; data were obtained by using a fiber optical instruments from Ocean Optics. The electrochemical cell was positioned between a tungsten halogen lamp and the detector, and the empty cell filled with electrolyte was taken as the 100% level of the transmittance; the calibration run was conducted before insertion of the sample in the electrolyte.

Acknowledgements

R.-T. Wen thankfully acknowledges useful discussions with M. Arvizu and C. Triana. The authors are grateful to D. Primetzhofer at the Division of Ion Physics at Uppsala University for Rutherford Backscattering Spectroscopy measurements. Financial support was received from the European Research Council under the European Community's Seventh Framework Program (FP7/2007-2013)/ERC Grant Agreement No. 267234 ("GRINDOOR").

Received: February 17, 2015
Revised: March 11, 2015
Published online: April 27, 2015

[1] C. G. Granqvist, *Handbook of Inorganic Electrochromic Materials*, Elsevier, Amsterdam, The Netherlands **1995**.
[2] C. G. Granqvist, *Nat. Mater.* **2006**, *5*, 89.
[3] G. A. Niklasson, C. G. Granqvist, *J. Mater. Chem.* **2007**, *17*, 127.
[4] C. G. Granqvist, *Thin Solid Films* **2014**, *564*, 1.
[5] D. Gillaspie, A. Norman, C. E. Tracy, J. R. Pitts, S.-H. Lee, A. Dillon, *J. Electrochem. Soc.* **2010**, *157*, H328.
[6] E. Amasawa, N. Sasagawa, M. Kimura, M. Taya, *Adv. Energy Mater.* **2014**, *4*, 1400379.
[7] H.-J. Yen, C.-J. Chen, G.-S. Liou, *Adv. Funct. Mater.* **2013**, *23*, 5307.
[8] E. S. Lee, S. E. Selkowitz, R. D. Clear, D. L. DiBartolomeo, J. H. Klems, L. L. Fernandes, G. J. Ward, V. Inkarojrit, M. Yazdanian, *California Energy Commission, PIER, CEC-500-2006-052*, **2006**.
[9] A. Jonsson, A. Roos, *Sol. Energy* **2010**, *84*, 1.
[10] A. Piccolo, *Energy Build.* **2010**, *42*, 1409.
[11] M. Pittaluga, in *Eco-Efficient Materials for Mitigating Building Cooling Needs: Design, Properties and Applications* (Eds: F. Pacheco-Torgal, J. Labrincha, L. F. Cabeza, C. G. Granqvist), Woodhead, Cambridge, UK **2015**, Ch. 17.
[12] J. S. E. M. Svensson, C. G. Granqvist, *Appl. Phys. Lett.* **1986**, *49*, 1566.
[13] E. Avendaño, A. Azens, G. A. Niklasson, C. G. Granqvist, *J. Electrochem. Soc.* **2005**, *152*, F203.
[14] E. Avendaño, H. Rensmo, A. Azens, A. Sandell, G. d. M. Azevedo, H. Siegbahn, G. A. Niklasson, C. G. Granqvist, *J. Electrochem. Soc.* **2009**, *156*, P132.
[15] H. Bode, K. Dehmelt, J. Witte, *Electrochim. Acta* **1966**, *11*, 1079.
[16] H. Bode, K. Dehmelt, J. Witte, *Z. Anorg. Allg. Chem.* **1969**, *366*, 1.

[17] S. Passerini, B. Scrosati, A. Gorenstein, *J. Electrochem. Soc.* **1990**, *137*, 3297.
[18] S. Passerini, B. Scrosati, *Solid State Ionics* **1992**, *53-56*, 520.
[19] F. Decker, S. Passerini, R. Pileggi, B. Scrosati, *Electrochim. Acta* **1993**, *37*, 1033.
[20] G. Campet, B. Morel, M. Bourrel, J. M. Chabagno, D. Ferry, R. Garie, C. Quet, C. Geoffroy, J. J. Videau, J. Portier, C. Delmas, J. Salardenne, *Mater. Sci. Eng. B* **1991**, *8*, 303.
[21] S. I. Cordoba-Torresi, C. Gabrielli, A. Hugot-Le Goff, R. Torresi, *J. Electrochem. Soc.* **1991**, *138*, 1548.
[22] S. Passerni, B. Scrosati, *J. Electrochem. Soc.* **1994**, *141*, 889.
[23] Y. G. Wu, G. M. Wu, X. Y. Ni, X. Wu, *Sol. Energy Mater. Sol. Cells* **2000**, *63*, 217.
[24] G. Boschloo, A. Hagfeldt, *J. Phys. Chem. B* **2001**, *105*, 3039.
[25] S. Green, J. Backholm, P. Georén, C. G. Granqvist, G. A. Niklasson, *Sol. Energy Mater. Sol. Cells* **2009**, *93*, 2050.
[26] S. V. Green, E. Pehlivan, C. G. Granqvist, G. A. Niklasson, *Sol. Energy Mater. Sol. Cells* **2012**, *99*, 339.
[27] F. Lin, D. Nordlund, T.-C. Weng, D. Sokaras, K. M. Jones, R. B. Reed, D. T. Gillaspie, D. G. J. Weir, R. G. Moore, A. C. Dillon, R. M. Richards, C. Engtrakul, *ACS Appl. Mater. Interfaces* **2013**, *5*, 3643.
[28] Y. Ren, W. K. Chim, L. Guo, H. Tanoto, J. Pan, S. Y. Chiam, *Sol. Energy Mater. Sol. Cells* **2013**, *116*, 83.
[29] M. Mihelčič, A. Š. Vuk, I. Jerman, B. Orel, F. Švegl, H. Moulki, C. Faure, G. Campet, A. Rougier, *Sol. Energy Mater. Sol. Cells* **2014**, *120*, 116.
[30] R.-T. Wen, C. G. Granqvist, G. A. Niklasson, *Appl. Phys. Lett.* **2014**, *105*, 163502.
[31] R.-T. Wen, G. A. Niklasson, C. G. Granqvist, *Thin Solid Films* **2014**, *565*, 128.
[32] H. Moulki, D. H. Park, B.-K. Min, H. Kwon, S.-J. Hwang, J.-H. Choy, T. Toupance, G. Campet, A. Rougier, *Electrochim. Acta* **2012**, *74*, 46.
[33] H. Moulki, C. Faure, M. Mihel i , A. Šurca Vuk, F. Švegl, B. Orel, G. Campet, M. Alfredsson, A. V. Chadwick, D. Gianolio, A. Rougier, *Thin Solid Films* **2014**, *553*, 63.
[34] S. Passerini, B. Scrosati, A. Gorenstein, A. M. Andersson, C. G. Granqvist, *J. Electrochem. Soc.* **1989**, *136*, 3394.
[35] T. Kubo, Y. Nishikitani, Y. Sawai, H. Iwanaga, Y. Sato, Y. Shigesato, *J. Electrochem. Soc.* **2009**, *156*, H629.
[36] R. C. Tenent, D. T. Gillaspie, A. Miedaner, P. A. Parilla, C. J. Curtis, A. C. Dillon, *J. Electrochem. Soc.* **2010**, *157*, H318.
[37] F. Lin, D. Nordlund, T.-C. Weng, R. G. Moore, D. T. Gillaspie, A. C. Dillon, R. M. Richards, C. Engtrakul, *ACS. Appl. Mater. Interfaces* **2013**, *5*, 301.
[38] C.-C. Wu, C.-F. Yang, *Nanoscale Res. Lett.* **2013**, *8*, 33.
[39] S. Passerini, J. Scarminio, B. Scrosati, D. Zane, F. Decker, *J. Appl. Electrochem.* **1993**, *23*, 1187.
[40] P. M. M. C. Bressers, E. A. Meulenkamp, *J. Electrochem. Soc.* **1998**, *145*, 2225.
[41] P. Poizot, S. Laruelle, S. Grugeon, L. Dupont, J.-M. Tarascon, *Nature* **2000**, *407*, 496.
[42] P. Poizot, S. Laruelle, S. Grugeon, J.-M. Tarascon, *J. Electrochem. Soc.* **2002**, *149*, A1212.
[43] Å. Andersson, O. Hunderi, C. G. Granqvist, *J. Appl. Phys.* **1980**, *51*, 754.
[44] G. A. Niklasson, C. G. Granqvist, *J. Appl. Phys.* **1979**, *50*, 5500.
[45] D. Cappus, C. Xu, D. Erlich, B. Dillmann, C. A. Ventrice Jr., K. Al Shamery, H. Kuhlenbeck, H.-J. Freund, *Chem. Phys.* **1993**, *177*, 53.
[46] M. Mihelčič, A. Šurca Vuk, I. Jerman, D. Vrhovšek, F. Švegl, M. Hajzeri, B. Orel, *Acta Chim. Slov.* **2014**, *61*, 517.
[47] M. Mihelčič, V. Francetič, P. Pori, H. Gradišar, J. Kovač, B. Orel, *Appl. Surf. Sci.* **2014**, *313*, 484.
[48] M. Ohring, *Materials Science of Thin Films*, 2nd ed., Academic, New York, NY **2002**.
[49] D. M. Mattox, *Handbook of Physical Vapor Deposition (PVD) Processing*, 2nd ed., Elsevier, Norwich, NY **2010**.
[50] B. D. Cullity, S. R. Stock, *Elements of X-ray Diffraction*, 3rd ed., Prentice-Hall, Upper Saddle River, NJ **2001**.
[51] H. Sato, T. Minami, S. Takata, T. Yamada, *Thin Solid Films* **1993**, *236*, 27.
[52] H. W. Ryu, G. P. Choi, W. S. Lee, J. S. Park, *J. Mater. Sci.* **2004**, *39*, 4375.
[53] H. L. Chen, Y. M. Lu, J. Y. Wu, W. S. Hwang, *Mater. Trans.* **2005**, *46*, 2530.
[54] J. E. B. Randles, *Trans. Faraday Soc.* **1948**, *44*, 327.
[55] A. Ševčík, *Collect. Czech. Chem. Commun.* **1948**, *13*, 349.
[56] M. Strømme, G. A. Niklasson, C. G. Granqvist, *Phys. Rev. B* **1995**, *52*, 14192.
[57] M. Strømme, G. A. Niklasson, C. G. Granqvist, *Phys. Rev. B* **1996**, *54*, 2968.
[58] M. Strømme, G. A. Niklasson, C. G. Granqvist, *Phys. Rev. B* **1996**, *54*, 17884.
[59] M. A. Langell, M. H. Nassir, *J. Phys. Chem. B* **1995**, *99*, 4162.
[60] F. Švegl, A. Šurca Vuk, M. Hajzeri, L. Slemenik Perše, B. Orel, *Sol. Energy Mater. Sol. Cells* **2012**, *99*, 14.
[61] M. Mayer, *Am. Inst. Phys. Conf. Proc.* **1999**, *475*, 541.
[62] R.-T. Wen, G. A. Niklasson, C. G. Granqvist, *Sol. Energy Mater. Sol. Cells* **2014**, *120*, 151.